2011 50th IEEE Conference on Decision and Control and
European Control Conference (CDC-ECC)
Orlando, FL, USA, December 12-15, 2011

A Dual-Model Fault Detection Approach with Application to Actuators of Robot Manipulators

Tesheng Hsiao, *Member, IEEE*, and Mao-Chiao Weng

***Abstract*— Multiple-model (MM)-based methods have been successfully applied to many fault detection schemes; however systematic design of the associated model set remains an open question. The difficulty comes from the fact that using a large model set reduces the risk of undetected faults, but also increases the computation load drastically. In this paper we propose a dual-model fault detection (DMFD) algorithm aiming at solving the model set design problem, and apply it to detect actuator faults of robot manipulators. The DMFD algorithm is able to detect various types of *unexpected* actuator faults, including abrupt faults, incipient faults, and simultaneous faults, in a computationally efficient way. To evaluate the performance of the DMFD algorithm, upper bounds of the false alarm and missed detection probabilities are explicitly presented in terms of the tunable variables. Furthermore, experiments are conducted to demonstrate its ability in immediate detection of faults.**

I. INTRODUCTION

Recent advances in intelligent robots have inspired many emerging applications that require close interactions with humans. Therefore it becomes crucial to guarantee safe operation of robots, especially in the presence of faults. To meet the stringent fail-safe requirement, a robotic system must be able to detect the occurrence of faults and responds appropriately.

In the literature of fault detection, faults are represented as either additive signals [1, 2] or multiple models [3-8]. The latter represents each fault by a specific model that might be simple and structurally different from one another; thus the multiple-model (MM) fault representation is flexible and powerful, leading to the recent development of MM-based fault detection schemes.

For example, eight fault models were established for the air-intake system of a turbo-charged engine [3]; then structured hypothesis tests were used to detect the occurrence of faults. The multiple model adaptive estimation (MMAE) algorithm, which runs parallel state estimators and calculates the probability of each model by Bayes' rule, has been applied to the flight control system [4]. To improve the performance of MM-based fault detection schemes, the interacting multiple model (IMM) algorithm was investigated [5] and applied to the satellite's attitude control system [6] as well as the aircraft lateral motion control system [7].

In principle, the set of fault models in the MM-based methods should contain all possible faults. If an *unexpected* fault, i.e. a fault without a corresponding model in the model set, has occurred, the results of the MM-based methods become unpredictable. However, in practice, the model set must be finite and thus can never be exhaustive. Moreover, the computation load increases drastically as the size of the model set increases. Therefore MM-based methods face a dilemma of avoiding unexpected faults by using a fine-grained model set while maintaining a tractable algorithm by limiting the size of the model set.

To tackle the model set design problem, Ru and Li [8] proposed the IM^{3}L algorithm that uses the IMM algorithm for estimating system state and the expectation-maximization (EM) algorithm for updating model parameters. Therefore the fault models are self-adaptive, relieving the need for a large model set. However only (multiple) abrupt total and partial faults were considered in [8].

In this paper, we propose the dual-model fault detection (DMFD) algorithm aiming at solving the model set design problem, and apply it to detect actuator faults of robot manipulators. The DMFD algorithm is able to detect various types of *unexpected* actuator faults, including abrupt faults, incipient faults, and simultaneous faults in a computationally efficient way. We also evaluate the upper bounds of the false alarm and missed detection probabilities in terms of tunable variables of the DMFD algorithm. Then experiments are carried out to verify the effectiveness of the DMFD algorithm.

The remainder of this paper is organized as follows: Section II introduces the dynamic and kinematic models of the robot manipulator. Section III illustrates the DMFD algorithm. Experimental results are presented in Section IV, and Section V concludes this paper.

II. Dynamic and Kinematic Models of the Manipulator

The dynamic model of an n-joint manipulator is [9]:

$$\mathbf{M}(\mathbf{q}(t))\ddot{\mathbf{q}}(t)+\mathbf{C}(\mathbf{q}(t),\dot{\mathbf{q}}(t))\dot{\mathbf{q}}(t)+\mathbf{G}(\mathbf{q}(t))+\mathbf{F}(\dot{\mathbf{q}}(t))=\boldsymbol{\tau}(t) \qquad (1)$$

where $\mathbf{q}(t), \dot{\mathbf{q}}(t), \ddot{\mathbf{q}}(t) \in \mathbb{R}^n$ are vectors of joint positions, velocities, and accelerations at time t, respectively. $\mathbf{M}(\mathbf{q}(t))$, $\mathbf{C}(\mathbf{q}(t),\dot{\mathbf{q}}(t)) \in \mathbb{R}^{n\times n}$ are the inertia matrix, and Coriolis and centrifugal matrix respectively. $\mathbf{G}(\mathbf{q}(t))$, $\mathbf{F}(\dot{\mathbf{q}}(t))$, $\boldsymbol{\tau}(t) \in \mathbb{R}^n$ denote the gravitational torque vector, friction vector, and control torque vector, respectively.

Define the state vector of the manipulator as

Tesheng Hsiao* is with the Department of Electrical Engineering, National Chiao Tung University, Hsinchu, 30010, Taiwan (TEL: 886-3-5131249; FAX: 886-3-5715998; e-mail: tshsiao@cn.nctu.edu.tw).

Mao-Chiao Weng is with the Institute of Electrical and Control Engineering, National Chiao Tung University, Hsinchu, 30010, Taiwan (e-mail: mcw615@ ymail.com).

$\mathbf{x} = [\mathbf{q}^T, \dot{\mathbf{q}}^T]^T$; then the discrete-time state space representation of (1) is:

$$\mathbf{x}_{k+1} = \mathbf{x}_k + h\begin{bmatrix} \dot{\mathbf{q}}_k \\ \mathbf{f}(\mathbf{x}_k, \boldsymbol{\tau}_k) \end{bmatrix} + \begin{bmatrix} \mathbf{w}_k^p \\ \mathbf{w}_k^v \end{bmatrix} \quad (2)$$

where the subscript k denotes the k^{th} time step, $\mathbf{f}(\mathbf{x}_k, \boldsymbol{\tau}_k) = \mathbf{M}^{-1}(\mathbf{q}_k)\left[\boldsymbol{\tau}_k - \mathbf{C}(\mathbf{q}_k, \dot{\mathbf{q}}_k)\dot{\mathbf{q}}_k - \mathbf{G}(\mathbf{q}_k) - \mathbf{F}(\dot{\mathbf{q}}_k)\right]$, h is the sampling time, and $\mathbf{w}_k = [(\mathbf{w}_k^p)^T, (\mathbf{w}_k^v)^T]^T$ is the process noise representing the model uncertainties and the approximation error incurred in discretizing (1).

We assume that only the joint positions are measurable. Thus the output equation of the manipulator is

$$\mathbf{y}_k = \mathbf{C}\mathbf{x}_k + \mathbf{v}_k \quad (3)$$

where $\mathbf{C}=[\mathbf{I}_{n\times n}\ \mathbf{0}_{n\times n}]$ and $\mathbf{v}_k$ is the measurement noise which is assumed to be Gaussian distributed white noise with zero mean and covariance matrix $\mathbf{R}$.

In the context of the DMFD algorithm, the *dynamic model* consists of (2) and (3) along with the assumption that $\mathbf{w}_k$ is zero mean Gaussian distributed with covariance matrix $\mathbf{Q}_k^D$.

Remark 1: It should be noted that the actual distribution of $\mathbf{w}_k$ may not be Gaussian; nevertheless the dynamic model *assumes* that $\mathbf{w}_k$ is Gaussian distributed and treats the covariance matrix $\mathbf{Q}_k^D$ as a *tunable parameter of the dynamic model*, not a *physical quantity of the manipulator*. In other words, we change the "accuracy" of the dynamic model by tuning $\mathbf{Q}_k^D$. If $\mathbf{Q}_k^D$ is set to an inappropriate value, then the dynamic model behaves poorly in predicting the motion of the manipulator; however, it is our intention to reduce the "relative accuracy" of one model w.r.t. the other for the purpose of fault detection. See Section III for more details.

We can also predict the motion of the manipulator through the *kinematic relations* of joints. By kinematic relations we mean that the joint velocity is the first derivative of the joint position. The kinematic relation can be approximated by the Euler's method as well as the backward difference equation; thus the following equation holds:

$$\mathbf{x}_{k+1} = \mathbf{A}^K\mathbf{x}_k + \mathbf{G}^K\boldsymbol{\xi}_k \quad (4)$$

where $\mathbf{A}^K = \begin{bmatrix} \mathbf{I} & h\mathbf{I} \\ \mathbf{0} & \mathbf{I} \end{bmatrix}$, $\mathbf{G}^K = \begin{bmatrix} \mathbf{I} & \mathbf{0} \\ \frac{1}{h}\mathbf{I} & \mathbf{I} \end{bmatrix}$, and $\boldsymbol{\xi}_k = \begin{bmatrix} \boldsymbol{\xi}_k^p \\ \boldsymbol{\xi}_k^v \end{bmatrix}$.

$\boldsymbol{\xi}_k^p$ and $\boldsymbol{\xi}_k^v$ are the approximation errors due to the Euler's method and the backward difference equation respectively.

In the context of the DMFD algorithm, the *kinematic model* consists of (4) and (3) along with the assumption that $\boldsymbol{\xi}_k$ is Gaussian distributed with zero mean and covariance matrix $\mathbf{Q}_k^K$. Here $\mathbf{Q}_k^K$ is also regarded as a tunable parameter of the kinematic model (c.f. Remark 1). Besides, we assume that $\mathbf{v}_k$, $\mathbf{w}_k$ and $\boldsymbol{\xi}_k$ are independent.

III. Dual-Model Fault Detection Algorithm

A. MM-based Fault Detection Schemes

The model set of the MM-based method contains all fault models and the *normal model*, i.e. (2), which implies that the robot is under normal operation. We say that the manipulator is currently in mode i if the i^{th} model in the model set best fits the current behavior (from the input-output point of view) of the manipulator.

Suppose that there are L models in the model set. Let $P(M_k^i)$ be the probability of the event M_k^i, which means that the manipulator is in mode i at step k, i=1,2,...,L, and $\forall k$. We assume that M_k^i forms a Markov chain, i.e. for i,j=1, 2,…,L and $\forall k$

$$P(M_{k+1}^j \mid M_k^i, M_{k-1}^{i_{k-1}}, \cdots M_0^{i_0}) = P(M_{k+1}^j \mid M_k^i) = \pi^{i,j} \quad (5)$$

$\pi^{i,j}$ is the *mode transition probability* satisfying $\sum_{j=1}^{L}\pi^{i,j} = 1$ for i=1,…,L. The *posterior mode probability* conditioning on all measurements up to step k is

$$s_k^i = P\left(M_k^i \mid \mathbf{y}_{1,}\mathbf{y}_{2,}\cdots\mathbf{y}_k\right), \quad i=1,2,\ldots L \text{ and } \forall k \quad (6)$$

If $s_k^j = \max\left\{s_k^1, \cdots s_k^L\right\}$, then we conclude that the manipulator is in mode j at step k. Furthermore, if mode j is associated with a particular fault, then we infer that the corresponding fault has taken place. Therefore the problem of fault detection is equivalent to evaluating the posterior mode probabilities (6).

Some useful techniques have been proposed to calculate (6). In this paper we use the *generalized pseudo Bayesian method of order 2* (GPB-2) [10] because it achieves a better performance. But its computation load is demanding. If there are L models in the model set, then at each time step, the GPB-2 algorithm should run L^2 state estimators each of which is based on one of the L models in the model set. Besides, the state estimators also calculate the following *likelihood functions*:

$$L_k^{i,j} = p\left(\mathbf{y}_k \mid \mathbf{y}_1, \cdots \mathbf{y}_{k-1}, M_{k-1}^i, M_k^j\right), i,j,=1,2,\ldots,L \quad (7)$$

where $p(\cdot)$ denotes the probability density function (PDF). According to the information provided by the state estimators, the GPB-2 algorithm assesses the posterior mode probability of each model. The better a model can predict the behavior of the manipulator, the higher its posterior mode probability will be.

B. Basic Concepts of the DMFD algorithm

As we have mentioned in Section I, design of the model set is the most challenging part of the MM-based fault detection schemes. To solve the model set design problem, we propose a dual-model fault detection (DMFD) algorithm which contains only two models in the model set: the dynamic model and the kinematic model. Recall that state estimators based on these two models are required; therefore we implement the unscented Kalman filter (UKF) [11] for the nonlinear dynamic model and the standard Kalman filter for the kinematic model. Then the GPB-2 algorithm is

applied to evaluate the posterior mode probabilities.

The idea behind the DMFD algorithm is easy to understand. Roughly speaking, we purposely increase $\mathbf{Q}_k^K$ or decrease $\mathbf{Q}_k^D$ such that the dynamic model is more "accurate" than the kinematic model under normal operation. Consequently, the GPB-2 algorithm favors the dynamic model and assigns a higher posterior mode probability to it, indicating that the manipulator is normal.

In the event of actuator faults, the faulty joints no longer satisfy the dynamic model; however the kinematic model remains a good approximation to the motion of all joints because it has nothing to do with actuators' torques. Thus the posterior mode probability of the kinematic model increases. If the posterior mode probability of the kinematic model exceeds a predefined threshold T_D, we assert the occurrence of faults. Note that $T_D \in (0,1)$ can be viewed as the least confidence level we must have when we claim that the manipulator has failed.

The advantages of the DMFD algorithm are apparent. Firstly, the DMFD algorithm does not incorporate any particular fault information into the models. Thus it is able to detect various unexpected faults provided that the faulty system deviates from the dynamic model far enough to lower down its posterior mode probability. Secondly, the DMFD algorithm is computationally efficient since only two models are involved in the model set.

C. Analysis of the DMFD Algorithm

According to the assumptions of the dynamic model and the kinematic model, the likelihood function $L_k^{i,j}$ defined in (7) is a Gaussian function, $i,j=D,K$. However, the *true* likelihood function, i.e. the PDF of $\mathbf{y}_k$ conditioning on $\mathbf{y}_1,\ldots\mathbf{y}_{k-1}$, is unknown and susceptible to faults. Let L_k^N and L_k^F denote the true likelihood functions under normal and faulty operating conditions respectively, i.e.

$$L_k^N = p\left(\mathbf{y}_k \mid \mathbf{y}_1,\cdots,\mathbf{y}_{k-1}, \text{the system is normal at step } k\right)$$
$$L_k^F = p\left(\mathbf{y}_k \mid \mathbf{y}_1,\cdots,\mathbf{y}_{k-1}, \text{the system is faulty at step } k\right)$$

L_k^N and L_k^F are unknown and may not be Gaussian. Their means and covariance matrices are denoted by $\boldsymbol{\mu}_k^N$, $\boldsymbol{\mu}_k^F$ and $\mathbf{S}_k^N$, $\mathbf{S}_k^F$, respectively, and are unknown either. We explicitly distinguish $L_k^{i,j}$, $i,j=D,K$, from L_k^N and L_k^F to emphasize the difference between *models* and the *physical system* because the accuracy of the models are purposely reduced.

Lemma 1: For any $k \in \mathbb{N}$, if we choose

$$\mathbf{Q}_k^i = \begin{bmatrix} \mathbf{Q}_{11,k}^i & \mathbf{0} \\ \mathbf{0} & \mathbf{Q}_{22,k}^i \end{bmatrix}, \quad i=D,K, \quad \text{and} \quad \mathbf{Q}_{11,k}^D = \mathbf{Q}_{11,k}^K \triangleq \mathbf{Q}_{11,k} \tag{8}$$

where $\mathbf{Q}_{11,k}^i, \mathbf{Q}_{22,k}^i \in \mathbb{R}^{n\times n}$, then $L_{k+1}^{i,D}\left(\mathbf{y}_{k+1}\right) = L_{k+1}^{i,K}\left(\mathbf{y}_{k+1}\right)$ for $i=D$, K, and all $\mathbf{y}_{k+1} \in \mathbb{R}^n$.

To prove Lemma 1, just substitute the dynamic model and the kinematic model into the UKF and the Kalman filter, respectively. Then we can find that under the condition of (8), the conclusion of Lemma 1 holds. Because the proof is straightforward, it is skipped to save the space.

If (8) holds for all k, then we define $L_k^i \triangleq L_k^{i,D} = L_k^{i,K}$ for $i=D,K$ and all k, and denote the mean and covariance matrix of L_k^i as $\boldsymbol{\mu}_k^i$ and $\mathbf{S}_k^i$ respectively. Furthermore, if we choose the mode transition probabilities defined in (5) to be $\pi^{D,D}=\pi^{K,K}=\pi^0$ and substitute L_k^i into the GPB-2 algorithm, then we have the following fault detection criterion:

The fault is detected at step k

$$\Leftrightarrow\ s_k^K \geq T_D \quad \Leftrightarrow \quad \frac{s_{k-1}^K L_k^K}{s_{k-1}^D L_k^D} \geq \frac{\pi^0-(1-T_D)}{\pi^0-T_D} \quad \Leftrightarrow \quad \upsilon_k \geq r$$

where $\upsilon_k = \rho_{k-1} + l_k$, $\rho_{k-1} = \log\frac{s_{k-1}^K}{s_{k-1}^D}$, $l_k = \log\frac{L_k^K}{L_k^D}$, and $r = \log\frac{\pi^0-(1-T_D)}{\pi^0-T_D}$.

l_k is the log likelihood ratio of the kinematic model to the dynamic model. Therefore if (8) holds, the DMFD algorithm is equivalent to the likelihood ratio test with a time-varying threshold r-ρ_{k-1}, which depends on the ratio of posterior mode probabilities at the previous time step.

Since l_k is a function of $\mathbf{y}_k$, its mean and variance w.r.t. L_k^N (L_k^F) are denoted by $E^N[l_k]$ ($E^F[l_k]$) and $\mathrm{var}^N(l_k)$ ($\mathrm{var}^F(l_k)$) respectively. Let $0 < \lambda_{1,k}^i \leq \cdots \leq \lambda_{n,k}^i$ be the eigenvalues of $\mathbf{S}_k^i$ for $i=D,K$; then the following lemma gives the bounds of the $E^i[l_k]$ and $\mathrm{var}^i(l_k)$ for $i=N,F$.

Lemma 2: If (8) holds for all k, then for $i=N,F$, we have

$$\underline{E}_k^i \triangleq \frac{1}{2}\left(n\log\frac{\lambda_{1,k}^D}{\lambda_{n,k}^K} + \frac{tr\mathbf{S}_k^i + \left\|\Delta\boldsymbol{\mu}_k^{iD}\right\|^2}{\lambda_{n,k}^D} - \frac{tr\mathbf{S}_k^i + \left\|\Delta\boldsymbol{\mu}_k^{iK}\right\|^2}{\lambda_{1,k}^K} \right)$$
$$\leq E^i\left[l_k\right] \leq \frac{1}{2}\left(n\log\frac{\lambda_{n,k}^D}{\lambda_{1,k}^K} + \frac{tr\mathbf{S}_k^i + \left\|\Delta\boldsymbol{\mu}_k^{iD}\right\|^2}{\lambda_{1,k}^D} - \frac{tr\mathbf{S}_k^i + \left\|\Delta\boldsymbol{\mu}_k^{iK}\right\|^2}{\lambda_{n,k}^K} \right) \triangleq \overline{E}_k^i \tag{9}$$

where $\Delta\boldsymbol{\mu}_k^{ij} = \boldsymbol{\mu}_k^i - \boldsymbol{\mu}_k^j$ for $i=N,F$ and $j=D,K$. $\|\bullet\|$ is the Euclidian norm and $tr\bullet$ is the trace of a matrix. Furthermore, if L_k^N and L_k^F are Gaussian functions, then for $i=N,F$

$$\mathrm{var}^i(l_k) \leq \left(tr\mathbf{S}_k^i\right)^2\left(\frac{1}{\lambda_{1,k}^D}+\frac{1}{\lambda_{1,k}^K}\right)^2 + tr\mathbf{S}_k^i\left(\frac{\left\|\Delta\boldsymbol{\mu}_k^{iD}\right\|}{\lambda_{1,k}^D}+\frac{\left\|\Delta\boldsymbol{\mu}_k^{iK}\right\|}{\lambda_{1,k}^K}\right)^2 \triangleq \overline{V}_k^i \tag{10}$$

Direct computation leads to (9), while the proof of (10) is based on the results of [12]. Since the proof of Lemma 2 is tedious and provides little insights into the following analysis, it is skipped to save the space.

Remark 2: From UKF and the Kalman filter, we see that $\mathbf{S}_k^i$ depends on $\mathbf{Q}_k^i$. In other words, if $\mathbf{Q}_k^i$ increases, so does $\mathbf{S}_k^i$. Therefore we will treat $\lambda_{j,k}^i$, $i=D,K$ and $j=1,\ldots,n$, as tunable variables in the subsequent analysis.

Remark 3: In Lemma 2, L_k^N and L_k^F are assumed to be Gaussian; However it is also possible to find an upper bound of $\mathrm{var}^i(l_k)$, i=N,F, w.r.t. any other distributions [12]. We made the Gaussian assumption because it facilitates the derivation of the upper bound in terms of $\lambda_{j,k}^i$.

Let P_k^{MD} and P_k^{FA} denote the probabilities of *missed detections* and *false alarms* at step k, respectively. Suppose that $\mathfrak{R}_k=\{\mathbf{y}_k\in\mathbb{R}^n|\upsilon_k(\mathbf{y}_k)<r\}$`1 is the set of outputs that do not trigger the alarm. $\mathfrak{R}_k^C$ denotes the complement of $\mathfrak{R}_k$. Then P_k^{MD} and P_k^{FA} are:

$$\begin{aligned}P_k^{MD} &= P\left(\mathbf{y}_k\in\mathfrak{R}_k \mid \text{the system has failed, } \mathbf{y}_1,\cdots,\mathbf{y}_{k-1}\right)\\ &=\int_{\mathfrak{R}_k} L_k^F d\mathbf{y}_k = \int 1_{\mathfrak{R}_k} L_k^F d\mathbf{y}_k = E^F\left[1_{\mathfrak{R}_k}\right]\end{aligned}$$

$$\begin{aligned}P_k^{FA} &= P\left(\mathbf{y}_k\in\mathfrak{R}_k^C \mid \text{the system is normal, } \mathbf{y}_1,\cdots,\mathbf{y}_{k-1}\right)\\ &=\int_{\mathfrak{R}_k^C} L_k^N d\mathbf{y}_k = 1-E^N\left[1_{\mathfrak{R}_k}\right]\end{aligned}$$

where 1_S is the indicator function of the set S, i.e. $1_S(\mathbf{y}_k)=1$ if $\mathbf{y}_k\in S$, and $1_S(\mathbf{y}_k)=0$ if $\mathbf{y}_k\notin S$. The following theorem gives upper bounds of P_k^{MD} and P_k^{FA} in terms of (9) and (10).

Theorem 1: If (8) holds, $\pi^0>T_D>0.5$, and L_k^N and L_k^F are Gaussian functions for all k, then

$$P_k^{FA}\le\begin{cases}\bar{P}_k^{FA}, & E^N[l_k]<r-\rho_{k-1}\\ 1, & E^N[l_k]\ge r-\rho_{k-1}\end{cases},\quad P_k^{MD}\le\begin{cases}\bar{P}_k^{MD}, & E^F[l_k]>r-\rho_{k-1}\\ 1, & E^F[l_k]\le r-\rho_{k-1}\end{cases}$$

where

$$\begin{aligned}\bar{P}_k^{FA} &= 1-\frac{1}{2r^2}\left\{\left(\rho_{k-1}+\bar{E}_k^N-r\right)^2+\bar{V}_k^N+r^2\right.\\ &\left.-\sqrt{\left[\left(\rho_{k-1}+\bar{E}_k^N\right)^2+\bar{V}_k^N\right]\left[\left(\rho_{k-1}+\bar{E}_k^N-2r\right)^2+\bar{V}_k^N\right]}\right\}<1\end{aligned}$$

$$\begin{aligned}\bar{P}_k^{MD} &= 1-\frac{1}{2r^2}\left\{\left(\rho_{k-1}+\bar{E}_k^F-r\right)^2+\bar{V}_k^F+r^2\right.\\ &\left.-\sqrt{\left[\left(\rho_{k-1}+\bar{E}_k^F\right)^2+\bar{V}_k^F\right]\left[\left(\rho_{k-1}+\bar{E}_k^F-2r\right)^2+\bar{V}_k^F\right]}\right\}<1\end{aligned}$$

Proof: We derive the upper bound of P_k^{FA} in detail. The upper bound of P_k^{MD} can be obtained by the same procedure. Define $\mathfrak{M}_k=\{\mathbf{y}_k\in\mathbb{R}^n\,|\,\upsilon_k(\mathbf{y}_k)<0\}$. Since $\pi^0>T_D>0.5$, r is positive. Therefore $\mathfrak{M}_k\subseteq\mathfrak{R}_k$, $\int_{\mathfrak{M}_k}\upsilon_k L_k^N d\mathbf{y}_k = E^N\left[1_{\mathfrak{M}_k}\upsilon_k\right]<0$, and $\int_{\mathfrak{R}_k\setminus\mathfrak{M}_k}\upsilon_k L_k^N d\mathbf{y}_k\ge 0$. Besides, $E^N\left[1_{\mathfrak{M}_k}\right]\le E^N\left[1_{\mathfrak{R}_k}\right]$. Then

$$\begin{aligned}E^N\left[\upsilon_k\right] &= \int_{\mathfrak{M}_k}\upsilon_k L_k^N d\mathbf{y}_k+\int_{\mathfrak{R}_k\setminus\mathfrak{M}_k}\upsilon_k L_k^N d\mathbf{y}_k+\int_{\mathfrak{R}_k^C}\upsilon_k L_k^N d\mathbf{y}_k\\ &\ge E^N\left[1_{\mathfrak{M}_k}\upsilon_k\right]+r\left(1-E^N\left[1_{\mathfrak{R}_k}\right]\right)\end{aligned}\quad(11)$$

Apply Cauchy-Schwarz inequality to $E^N\left[1_{\mathfrak{M}_k}\upsilon_k\right]$ and rearrange (11); then we obtain

$$\psi\left(\sqrt{E^N\left[1_{\mathfrak{R}_k}\right]}\right)\triangleq rE^N\left[1_{\mathfrak{R}_k}\right]+\sqrt{E^N\left[\upsilon_k^2\right]}\sqrt{E^N\left[1_{\mathfrak{R}_k}\right]}+\left(E^N[\upsilon_k]-r\right)\ge 0$$

Note that ψ is a convex parabolic function of $\sqrt{E^N\left[1_{\mathfrak{R}_k}\right]}$. It is easy to show that ψ has two real roots and at least one of them is negative. Therefore if $E^N[\upsilon_k]\ge r$, both roots are negative, implying that $\psi\ge 0$ for all $0\le E^N\left[1_{\mathfrak{R}_k}\right]\le 1$. On the other hand, if $E^N[\upsilon_k]<r$, then we can show that ψ has one positive root which is always less than 1. Under these circumstances, $\psi\ge 0$ implies

$$\begin{aligned}0 &\le \frac{1}{2r}\left(-\sqrt{E\left[\upsilon_k^2\right]}+\sqrt{E^N\left[\upsilon_k^2\right]-4r\left(E^N[\upsilon_k]-r\right)}\right)\\ &\le\sqrt{E^N\left[1_{\mathfrak{R}_k}\right]}\le 1\end{aligned}\quad(12)$$

Since $P_k^{FA}=1-E^N\left[1_{\mathfrak{R}_k}\right]$, $E^N[\upsilon_k]\ge r$ implies the trivial upper bound, i.e. $P_k^{FA}\le 1$. On the other hand, if $E^N[\upsilon_k]<r$, from (12) we have

$$\begin{aligned}P_k^{FA} &\le 1-\frac{1}{2r^2}\left\{\left(\rho_k+E[l_k]-r\right)^2+\mathrm{var}^N(l_k)+r^2\right.\\ &\left.-\sqrt{\left[\left(\rho_k+E[l_k]\right)^2+\mathrm{var}^N(l_k)\right]\left[\left(\rho_k+E[l_k]-2r\right)^2+\mathrm{var}^N(l_k)\right]}\right\}\\ &\triangleq \hat{P}_k^{FA}\left(E^N[l_k],\mathrm{var}^N(l_k)\right)<1\end{aligned}$$

It is straightforward to show that the partial derivatives of $\hat{P}_k^{FA}$ w.r.t. both $E^N[l_k]$ and $\mathrm{var}^N(l_k)$ are always nonnegative, i.e. $\hat{P}_k^{FA}$ is a non-decreasing function of $E^N[l_k]$ and $\mathrm{var}^N(l_k)$. Because $E^N[l_k]$ and $\mathrm{var}^N(l_k)$ are upper bounded by $\bar{E}_k^N$ and $\bar{V}_k^N$ respectively, we conclude that $P_k^{FA}\le\hat{P}_k^{FA}\left(\bar{E}_k^N,\bar{V}_k^N\right)=\bar{P}_k^{FA}$ if $E^N[l_k]<r-\rho_{k-1}$, and $P_k^{FA}\le 1$ if $E^N[l_k]\ge r-\rho_{k-1}$. ■

According to Lemma 2 and Theorem 1, a sufficient condition for the existence of nontrivial upper bounds of both P_k^{FA} and P_k^{MD} is

$$\bar{E}_k^N<r-\rho_{k-1}<\underline{E}_k^F\quad(13)$$

Suppose that (13) holds; then we investigate the guidelines for tuning $\lambda_{j,k}^i$ to make $\bar{P}_k^{FA}$ and $\bar{P}_k^{MD}$ tighter upper bounds. By (9) and (10), $\bar{P}_k^{FA}$ and $\bar{P}_k^{MD}$ are functions of $\lambda_{1,k}^D$, $\lambda_{n,k}^D$, $\lambda_{1,k}^K$, and $\lambda_{n,k}^D$. We can show that $\frac{\partial\bar{P}_k^{FA}}{\partial\lambda_{n,k}^D}>0$, $\frac{\partial\bar{P}_k^{FA}}{\partial\lambda_{n,k}^K}>0$, $\frac{\partial\bar{P}_k^{FA}}{\partial\lambda_{1,k}^D}<0$, and $\frac{\partial\bar{P}_k^{FA}}{\partial\lambda_{1,k}^K}<0$. Therefore $\bar{P}_k^{FA}$ decreases whenever $\lambda_{n,k}^D$ and $\lambda_{n,k}^K$ decrease, and $\lambda_{1,k}^D$ and $\lambda_{1,k}^D$ increase. However, $\lambda_{1,k}^D\le\lambda_{n,k}^D$ and $\lambda_{1,k}^K\le\lambda_{n,k}^K$. Thus minimizing $\bar{P}_k^{FA}$ requires that

$$\lambda_{1,k}^D=\lambda_{n,k}^D\triangleq\lambda_k^D\quad\text{and}\quad\lambda_{1,k}^K=\lambda_{n,k}^K\triangleq\lambda_k^K\quad(14)$$

Similarly, (14) holds for $\bar{P}_k^{MD}$ to be minimal. Note that λ_k^D and λ_k^K are still undetermined.

On the other hand, if we choose $\lambda_{j,k}^i$, i=D,K and j=1,…,n, such that (14) holds, then (13) becomes

$$\frac{tr\mathbf{S}_k^N + \left\|\Delta\boldsymbol{\mu}_k^{ND}\right\|^2}{\alpha} - \left(tr\mathbf{S}_k^N + \left\|\Delta\boldsymbol{\mu}_k^{NK}\right\|^2\right) < \lambda_k^K\left[2\left(r-\rho_{k-1}\right) - n\log\alpha\right] \quad (15)$$
$$< \frac{tr\mathbf{S}_k^F + \left\|\Delta\boldsymbol{\mu}_k^{FD}\right\|^2}{\alpha} - \left(tr\mathbf{S}_k^F + \left\|\Delta\boldsymbol{\mu}_k^{FK}\right\|^2\right)$$

where $\alpha = \frac{\lambda_k^D}{\lambda_k^K}$. Suppose that

$$tr\mathbf{S}_k^N < tr\mathbf{S}_k^F,\ \left\|\Delta\boldsymbol{\mu}_k^{ND}\right\| < \left\|\Delta\boldsymbol{\mu}_k^{FD}\right\|, \text{ and } \left\|\Delta\boldsymbol{\mu}_k^{FK}\right\| < \left\|\Delta\boldsymbol{\mu}_k^{NK}\right\| \quad (16)$$

and $\alpha < \min\left\{1,\ \frac{tr\mathbf{S}_k^F + \left\|\Delta\boldsymbol{\mu}_k^{FD}\right\|^2}{tr\mathbf{S}_k^F + \left\|\Delta\boldsymbol{\mu}_k^{FK}\right\|^2},\ e^{\frac{2(r-\rho_{k-1})}{n}}\right\}$; then there exists $\lambda_k^K > 0$ that satisfies (15), or equivalently, (13). This implies that nontrivial upper bounds of both P_k^{FA} and P_k^{MD} exist.

Note that (16) means that failure of the system causes a larger variation in the output ($tr\mathbf{S}_k^N < tr\mathbf{S}_k^F$), the dynamic model is closer to the normal system ($\left\|\Delta\boldsymbol{\mu}_k^{ND}\right\| < \left\|\Delta\boldsymbol{\mu}_k^{FD}\right\|$), and the kinematic model is closer to the faulty system ($\left\|\Delta\boldsymbol{\mu}_k^{FK}\right\| < \left\|\Delta\boldsymbol{\mu}_k^{NK}\right\|$). The last two conditions of (16) just consolidate the basic concept of the DMFD algorithm in adjusting the "relative accuracy" between models.

Although it is desirable to find "optimal" λ_k^D and λ_k^K such that $\bar{P}_k^{FA}$ and $\bar{P}_k^{MD}$ are minimized, the optimization problem is not solvable because many unknown variables (e.g. $tr\mathbf{S}_k^i$ and $\left\|\Delta\boldsymbol{\mu}_k^{ij}\right\|$, i=N,F and j=D,K) are involved. Instead, the parameters of the DMFD algorithm are tuned on a trial and error basis in the experiments. Despite non-optimality of the parameters, experimental results show that the DMFD algorithm still performs well.

IV. Experiments

A. Experimental Setting

A two-joint manipulator on a vertical plane was set up for experimental verifications. Each link of the manipulator is driven by a DC motor with an optical encoder mounted on the shaft. The motion controller and the DMFD algorithm are implemented on a 32-bit floating point DSP chip (TMS320F28335) with sampling time 0.01sec. The dynamics of the DC motors and the manipulator are lumped together as follows [9]:

$$\begin{bmatrix} \theta_1+\theta_2+2\theta_3\cos q_2 & \theta_2+\theta_3\cos q_2 \\ \theta_7+\theta_8\cos q_2 & \theta_7+\theta_9 \end{bmatrix}\begin{bmatrix}\ddot{q}_1\\ \ddot{q}_2\end{bmatrix} + \begin{bmatrix} -\theta_3\dot{q}_2\sin q_2 & -\theta_3(\dot{q}_1+\dot{q}_2)\sin q_2 \\ \theta_8\dot{q}_1\sin q_2 & 0 \end{bmatrix}\begin{bmatrix}\dot{q}_1\\ \dot{q}_2\end{bmatrix}$$
$$+\begin{bmatrix} \theta_4\cos q_1 + \frac{g}{l_1}\theta_3\cos(q_1+q_2) \\ \frac{g}{l_1}\theta_8\cos(q_1+q_2)\end{bmatrix} + \begin{bmatrix}\theta_5\dot{q}_1+\theta_6\,\mathrm{sgn}\,\dot{q}_1 \\ \theta_{10}\dot{q}_1+\theta_{11}\,\mathrm{sgn}\,\dot{q}_1\end{bmatrix} = \begin{bmatrix} v_1\\ v_2\end{bmatrix}$$

where the control inputs v_1 and v_2 are armature voltages of the DC motors within the range of ±24 volts. θ_i, i=1,…,11, are model parameters explained in Table 1. Their values are determined by the system identification techniques [13], and are given in Table 1 too. SI unit system is adopted for all physical quantities of the manipulator which are shown in Table 2.

A robust motion controller is implemented on the manipulator such that the joint position follows a desired trajectory. In the experiments, the desired trajectory in the joint space is:

$$q_{1d}(t) = -\tfrac{\pi}{2} + \tfrac{\pi}{4}(1-e^{-2t^3}) + \tfrac{\pi}{9}(1-e^{-2t^3})\sin(4t)$$
$$q_{2d}(t) = \tfrac{\pi}{3}(1-e^{-2t^3}) + \tfrac{\pi}{6}(1-e^{-2t^3})\sin(3t)$$

Table 1: model parameters and their nominal values

$\theta_1 = [(I_1 + m_1 l_{c1}^2 + m_2 l_1^2)\frac{1}{r_1^2} + J_1]\frac{1}{k_1}$		0.3339	
$\theta_2 = (I_2 + m_2 l_{c2}^2)\frac{1}{r_1^2 k_1}$		$\theta_3 = m_2 l_1 l_{c2}\frac{1}{r_1^2 k_1}$	0.0054
$\theta_4 = (m_1 l_{c1} + m_2 l_1) g \frac{1}{r_1^2}\frac{1}{k_1}$	2.1450	$\theta_5 = b_1\frac{1}{k_1}$	2.8219
$\theta_6 = f_{c1}\frac{1}{r_1^2}\frac{1}{k_1}$	1.5177	$\theta_7 = (I_2 + m_2 l_{c2}^2)\frac{1}{r_2^2 k_2}$	0.0240
$\theta_8 = m_2 l_1 l_{c2}\frac{1}{r_2^2 k_2}$	0.0280	$\theta_9 = J_2\frac{1}{r_2^2 k_2}$	0.00002
$\theta_{10} = b_2\frac{1}{k_2}$	1.2211	$\theta_{11} = f_{c2}\frac{1}{r_2^2}\frac{1}{k_2}$	1.6282

Table 2: nomenclature of the model parameters

I_1, (I_2)	moment of inertia of the 1st (2nd) link
m_1, (m_2)	mass of the 1st (2nd) joint
l_1, (l_2)	length of the 1st (2nd) joint
l_{c1}, (l_{c2})	distance from the joint to the C.G. of the 1st (2nd) link
J_1, (J_2)	inertia of the motor's rotor of the 1st (2nd) joint
r_1, (r_2)	gear ratio of the 1st (2nd) joint
k_1, (k_2)	lumped constants of motors in the 1st (2nd) joint
f_{c1}, (f_{c2})	Coulomb friction coefficients of the 1st (2nd) joint
b_1, (b_2)	combined viscous friction coefficients
g	gravity acceleration

The following parameters of the DMFD algorithm are chosen:

$\mathbf{R}=0.001^2\mathbf{I}$, $\mathbf{Q}_{11,k}=0.0026^2\mathbf{I}$, $\mathbf{Q}_{22,k}^D=0.0023^2\mathbf{I}$, $\mathbf{Q}_{22,k}^K=0.003^2\mathbf{I}$, for all k, $\pi^{D,D}=\pi^{K,K}=0.999$, and $T_D=0.7$.

We have conducted extensive experimental tests to verify the ability of the DMFD algorithm in detecting various types of actuator faults, including abrupt faults, incipient faults, and simultaneous faults. Due to the limited space, only two types of faults in Table 3 are presented in this paper. Note that Type 1 fault is an abrupt simultaneous fault while Type 2 fault is an incipient fault indicating the gradual loss of the actuator's torque. In the experiments, the DMFD algorithm stops updating posterior mode probabilities once the fault has been detected. The frozen posterior mode probabilities indicate that the manipulator used to fail, no matter whether the fault persists or vanishes thereafter.

Note that it is difficult for the conventional MM-based method to model Type 2 fault since both the starting time and the time constant of the decay are uncertain. However, the DMFD algorithm can handle Type 2 fault easily.

Table 3: Types of actuator faults

Type	Description
Type 1	Both joints are locked simultaneously.
Type 2	The output torque of the 2nd joint gradually decays to zero with time constant 1/0.15 sec.

B. Experimental Results

- **Both joints are locked simultaneously (Type 1):**

Suppose that both joints are suddenly locked at t=7.2 sec. The positions, velocities, and armature voltages of both

joints are shown in Figure 1. Figure 2 illustrates the posterior mode probabilities. The DMFD algorithm detects the fault within 0.03 sec.

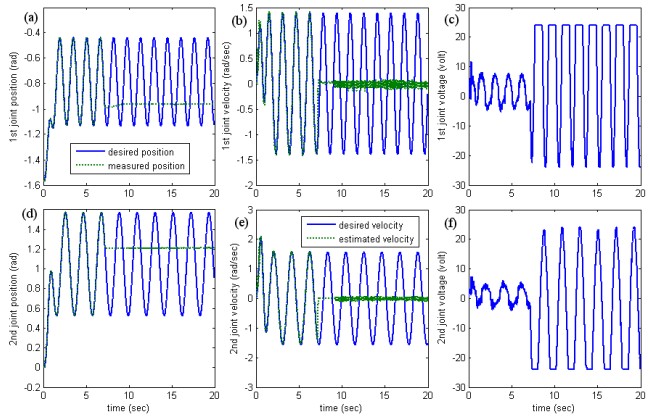

Figure 1: Both joints are locked at t=7.2sec. (a)(d) joint positions: solid line (-): desired trajectory; dotted line (.): real trajectory; (b)(e) joint velocities: solid line (-): desired velocities; dotted line (.): estimated velocities; (c)(f): armature voltages of both joints.

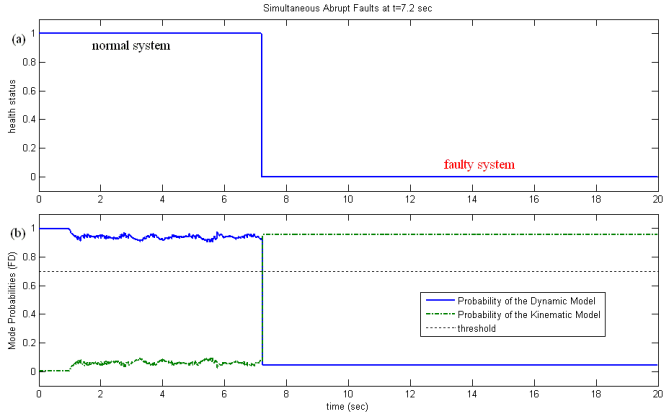

Figure 2: (a) The fault occurs suddenly at t=7.2sec. (b) posterior mode probabilities of the dynamic model (solid line) and the kinematic model (dashed line). The fault is detected at t=7.23 sec.

- **The output torque of the 2nd joint gradually decays (Type 2)**

Suppose that the output torque of the 2nd joint gradually decays after t=7 sec. More precisely, let τ_2 be the output torque delivered by the controller to the 2nd joint, and τ_{2a} be the actual torque experienced by the 2nd link. We assume that $\tau_{2a}(t) = e^{-0.15(t-7)}\tau_2(t)$ for $t \geq 7$. The results are shown in Figure 3.

Because the torque of the 2nd joint gradually decays, the controller gradually increases the armature voltage of the 2nd joint to compensate for the loss of the control torque. Therefore, the tracking performance degenerates slightly before the fault is detected and the DMFD algorithm takes a longer time (3.21 sec) to detect the fault. However we consider the detection delay as acceptable since no significant performance deterioration was observed during this delay time.

V. Conclusion

In this paper, we proposed the DMFD algorithm as a solution to the model set design problem, which is the most challenging part of the MM-based methods. By including only the dynamic model and the kinematic model into the model set, the DMFD algorithm is much more computationally efficient. In addition, it is applicable to various types of unexpected actuator faults, including abrupt faults, incipient faults, and simultaneous faults. Experiments were conducted on a two-joint robot manipulator. Experimental results verified the good performance of the DMFD algorithm.

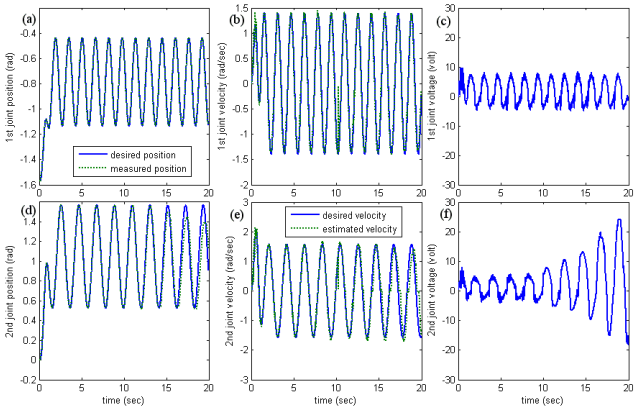

Figure 3: The output torque of the 2nd joint gradually decay, starting at t=7 sec. (a)(d) joint positions: solid line (-): desired trajectory; dotted line (.): real trajectory; (b)(e) joint velocities: solid line (-): desired velocities; dotted line (.): estimated velocities; (c)(f): armature voltages of both joints.

References

[1] M. L. Visinsky, *et al.*, "Robotic Fault Detection and Fault Tolerance: A Survey," *Reliability Engineering and System Safety,* vol. 46, pp. 139-158, 1994.

[2] W. E. Dixon, *et al.*, "Fault Detection for Robot Manipulators with Parametric Uncertainty: A Prediction-Error-Based Approach," *IEEE Transactions on Robotics and Automation,* vol. 16, pp. 689-699, 2000.

[3] M. Nyberg, "Model-Based Diagnosis of an Automotive Engine Using Several Types of Fault Models," *IEEE Transactions on Control Systems Technology,* vol. 10, pp. 679-689, 2002.

[4] T. E. Menke and P. S. Maybeck, "Sensor/Actuator Failure Detection in the Vista F-16 by Multiple Model Adaptive Estimation," *IEEE Transactions on Aerospace and Electronics Systems,* vol. 31, pp. 1218-1229, 1995.

[5] Y. Zhang and X. R. Li, "Detection and Diagnosis of Sensor and Actuator Failures Using IMM Estimator," *IEEE Transactions on Aerospace and Electronics Systems,* vol. 34, pp. 1293-1313, 1998.

[6] N. Tudoroiu and K. Khorasani, "Satellite Fault Diagnosis using a Bank of Interacting Kalman Filters," *IEEE Transactions on Aerospace and Electronic Systems,* vol. 43, pp. 1334-1350, 2007.

[7] S. Kim, *et al.*, "Fault Detection and Diagnosis of Aircraft Actuators using Fuzzy-Tuning IMM Filter," *IEEE Transactions on Aerospace and Electronic Systems,* vol. 44, pp. 940-952, 2008.

[8] J. Ru and X. R. Li, "Variable-Structure Multiple-Model Approach to Fault Detection, Identification, and Estimation," *IEEE Transactions on Control Systems Technology,* vol. 16, pp. 1029-1038, 2008.

[9] H. G. Sage, *et al.*, "Robust Control of Robot Manipulators: a Survey," *International Journal of Control,* vol. 72, pp. 1498-1522, 1999.

[10] Y. Bar-Shalom, *et al.*, *Estimation with Applications to Tracking and Navigation*: JOHN WILEY & SONS, INC., 2001.

[11] S. Thrun, *et al.*, *Probabilistic Robotics*: The MIT Press, 2005.

[12] T. Cacoullos, "On Upper and Lower Bounds for the Variance of a Function of a Random Variable," *The Annuals of Probability,* vol. 10, pp. 799-809, 1982.

[13] H. A. P. Blom and Y. Bar-Shalom, "The Interacting Multiple Model Algorithm for Systems with Markovian Switching Coefficients," *IEEE Transactions on Automatic Control,* vol. 33, pp. 780-783, 1998.